Monthly Notices
of the
ROYAL ASTRONOMICAL SOCIETY

MNRAS **469,** S636–S645 (2017)
Advance Access publication 2017 June 27

doi:10.1093/mnras/stx1620

The pebbles/boulders size distributions on Sais: *Rosetta*'s final landing site on comet 67P/Churyumov–Gerasimenko

M. Pajola,[1⋆] A. Lucchetti,[2⋆] M. Fulle,[3] S. Mottola,[4] M. Hamm,[4] V. Da Deppo,[5] L. Penasa,[6,7] G. Kovacs,[8] M. Massironi,[7] X. Shi,[8] C. Tubiana,[8] C. Güttler,[8] N. Oklay,[4] J. B. Vincent,[4] I. Toth,[9,10] B. Davidsson,[11] G. Naletto,[5,6,12] H. Sierks,[8] C. Barbieri,[6,13] P. L. Lamy,[14] R. Rodrigo,[15,16] D. Koschny,[17] H. Rickman,[18,19] H. U. Keller,[5,20] J. Agarwal,[8] M. F. A'Hearn,[21] M. A. Barucci,[22] J. L. Bertaux,[23] I. Bertini,[6] G. Cremonese,[2] S. Debei,[24] M. De Cecco,[25] J. Deller,[8] M. R. El Maarry,[26,27] S. Fornasier,[22] E. Frattin,[2,13] A. Gicquel,[8,11] O. Groussin,[9] P. J. Gutierrez,[28] S. Höfner,[8] M. Hofmann,[8] S. F. Hviid,[5] W. H. Ip,[29,30] L. Jorda,[9] J. Knollenberg,[5] J. R. Kramm,[8] E. Kührt,[5] M. Küppers,[31] L. M. Lara,[28] M. Lazzarin,[13] J. J. Lopez Moreno,[28] F. Marzari,[13] H. Michalik,[32] F. Preusker,[5] F. Scholten[5] and N. Thomas[26]

Affiliations are listed at the end of the paper

Accepted 2017 June 23. Received 2017 June 21; in original form 2017 March 30

ABSTRACT

By using the imagery acquired by the Optical, Spectroscopic, and Infrared Remote Imaging System Wide-Angle Camera (OSIRIS WAC), we prepare a high-resolution morphological map of the *Rosetta* Sais final landing site, characterized by an outcropping consolidated terrain unit, a coarse boulder deposit and a fine particle deposit. Thanks to the 0.014 m resolution images, we derive the pebbles/boulders size-frequency distribution (SFD) of the area in the size range of 0.07–0.70 m. Sais' SFD is best fitted with a two-segment differential power law: the first segment is in the range 0.07–0.26 m, with an index of -1.7 ± 0.1, while the second is in the range 0.26–0.50 m, with an index of $-4.2\ ^{+0.4}_{-0.8}$. The 'knee' of the SFD, located at 0.26 m, is evident both in the coarse and fine deposits. When compared to the Agilkia Rosetta Lander Imaging System images, Sais surface is almost entirely free of the ubiquitous, cm-sized debris blanket observed by Philae. None the less, a similar SFD behaviour of Agilkia, with a steeper distribution above ∼0.3 m, and a flatter trend below that, is observed. The activity evolution of 67P along its orbit provides a coherent scenario of how these deposits were formed. Indeed, different lift pressure values occurring on the two locations and at different heliocentric distances explain the presence of the cm-sized debris blanket on Agilkia observed at 3.0 au inbound. Contrarily, Sais activity after 2.1 au outbound has almost completely eroded the fine deposits fallen during perihelion, resulting in an almost dust-free surface observed at 3.8 au.

Key words: methods: data analysis – methods: statistical – comets: individual (67P C–G).

1 INTRODUCTION

On 2016 September 30, after 26 months investigating comet 67P/Churyumov–Gerasimenko, hereafter 67P, the European Space Agency *Rosetta* mission came to an end. Instead of putting the spacecraft into hibernation again, with uncertain consequences on the aging instruments, it was preferred to set *Rosetta* on a collision course with the comet, maximizing the scientific return by performing unprecedented measurements at increasing vicinity to the nucleus. The landing site targeted for the final descent was Sais, a region on the small lobe of 67P in close proximity to one of the active pits presented in Vincent et al. (2015) in the Ma'at region

⋆ E-mail: maurizio.pajola@gmail.com, maurizio.pajola@nasa.gov (MP); alice.lucchetti@oapd.inaf.it (AL)

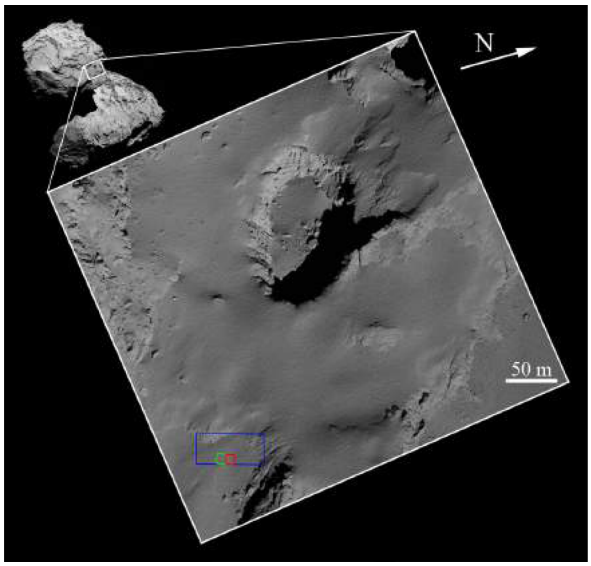

Figure 1. Context image showing the location of the *Rosetta* Sais landing site on the small lobe of 67P. The blue rectangle shows the extension of Fig. 3, while the green and red squares show the location of Fig. 4. The N arrow shows the direction of north. (For interpretation of the references to colour in this figure legend, the reader is referred to the web version of this article.)

(El-Maarry et al. 2015; Thomas et al. 2015b), Fig. 1. Eventually, once *Rosetta* flew over the mentioned pit, it redirected the Optical, Spectroscopic, and Infrared Remote Imaging System (OSIRIS; Keller et al. 2007) over the ultimate landing spot, returning some of the highest resolution images ever obtained from a planetary spacecraft.

The final OSIRIS data set sent back to Earth is comparable in resolution with the one obtained by the Philae/Rosetta Lander Imaging System (ROLIS) camera while landing on 67P (Mottola et al. 2015). Therefore, it provided the possibility to perform the same surface analysis Philae descent permitted to do, focusing on surface texture, pebbles/boulders identification and high-resolution morphological mapping. In this way, we had the unique opportunity to compare the Sais results with the Agilkia ones (Pajola et al. 2016a), i.e. we could compare the pebbles/boulders distribution in two completely different locations with different surface evolution on 67P.

Such analysis is part of a larger effort with the following aims: (i) to derive the pebbles/boulders size-frequency distributions (SFDs) from different locations and with different scales on 67P, (ii) to derive the possible formation/degradation processes that lead to such distributions (Pajola et al. 2015, 2016b,c) and (iii) to insert them in the wider context of cometary boulders (Pajola et al. 2016d) research.

In most cometary papers, the word dust is used to define all the refractory component leaving the nucleus surface. In comet 103P/Hartley 2, dust was releasing ≈80 per cent of the water gas in the coma, so that this dust must have some ice fraction inside it (Fulle et al. 2016a). However, since the total cross-section of the dust in the coma is much larger than the nucleus cross-section, this fact does not constrain the actual ice content of dust. In 67P, the water gas released by dust is <5 per cent of the total water loss (Fulle et al. 2016a), and the 67P northern deposits constrain the ice mass fraction of dust to ≈5 per cent as well (Fulle et al. 2017), so that in first approximation the 67P dust is ice-free. In this paper, we define dust as the refractory particles smaller than the resolution of the analysed images, all other refractory particles are named pebbles or boulders, according to their size, as specified in Pajola et al. (2016a).

The work is structured as follows: after the description of the OSIRIS data set and methods, we will focus on the results obtained on the surface of Sais. The resulting pebbles/boulders SFDs will then be compared to the Agilkia Philae observations. Finally, the implications on 67P's cometary regolith and the dust lifting processes will be presented, contextualizing them with different locations on 67P.

2 DATA SET AND METHODS

The OSIRIS instrument was composed by a Narrow-Angle Camera (NAC) and a Wide-Angle Camera (WAC) with a field of view (FOV) of 2.35° × 2.35° and 11.35° × 12.11°, respectively. Despite having the NAC camera A scale factor ∼5.4 larger than the WAC (18.8 mm pixel^{-1} when it was at 1 km from the surface versus the WAC scale of 101.5 mm pixel^{-1} at the same distance), it was out of focus for distances ≤1 km from the target.[1] On the contrary, the WAC camera was designed to stay in focus from 500 m to infinity, however, the focus degradation for the WAC was minimal also for distances down to 100 m, and by using the clear filter position on the filter wheel it could stay in a reasonably good focus[2] also for distances between 10 and 20 m. For this reason, the final set of OSIRIS highest resolution images taken during the *Rosetta* landing day were the WAC ones. The analysis we present here is therefore based on three WAC images taken on 2016 September 30. The observation geometries, scales, phase angles and FOVs of such images are presented in Table 1. We point out that the distortion of the WAC instrument is quite large, but since in this paper we are measuring the size of pebbles/boulders, we are working on distortion-corrected Level 3 images produced and validated through the OSIRIS pipeline (Tubiana et al. 2015).

The first WAC image of Table 1 was imported into the ARCGIS 10.1 software to distinguish and outline the different morphological units present on Sais. Out of the entire data set, this image was selected and used because it is the one with the highest resolution (scale factor of 4.57 cm pixel^{-1}) and that provides the widest context for our analysis. Contrarily, the other two WAC images of Table 1 were used to identify the pebbles/boulders[3] present on the different terrains of the Sais landing site. Such identification was manually performed through the ARCGIS 10.1 software. First, the pebbles/boulders were visually identified based on their shape, their appearance with respect to the background and on the presence of a shadow. Then, their outline was approximated by a polygon, extracting their areas and returning the linear metric size as the diameter of a circle with the same area as the polygon itself. Given the ∼ 0.014 m pixel^{-1}

[1] For the NAC case, the filter wheels contained antiradiation-coated plates of varying thickness, allowing two different focusing ranges: far focus (infinity to 2 km, optimized at 4 km) and near focus (2 km to 1 km, optimized at 1.3 km).

[2] This configuration was never used before during the entire *Rosetta* mission, but proved to work correctly during the final landing day.

[3] Following the official USGS size terms after Wentworth (1922), 'boulders' have diameters >0.25 m, 'cobbles' range between 0.25 and 0.064 m, while 'pebbles' sizes range between 0.064 and 0.002 m. Following the Pajola et al. (2016a) work, we decided to call all particles with diameters <0.25 m 'pebbles', while we named those >0.25 m as 'boulders'.

Table 1. The three OSIRIS WAC images used for the presented analysis. They were taken when 67P was at 3.82 au from Sun.

Date	UT	Distance (m)	Scale (m pixel^{-1})	Phase angle (°)	Field of view (m)
2016-09-30	10:30:38	452.16	0.046	31.32	74.58 × 29.25
2016-09-30	10:36:55	138.24	0.014	30.54	9.38 × 9.38
2016-09-30	10:37:04	130.46	0.013	30.53	8.85 × 8.85

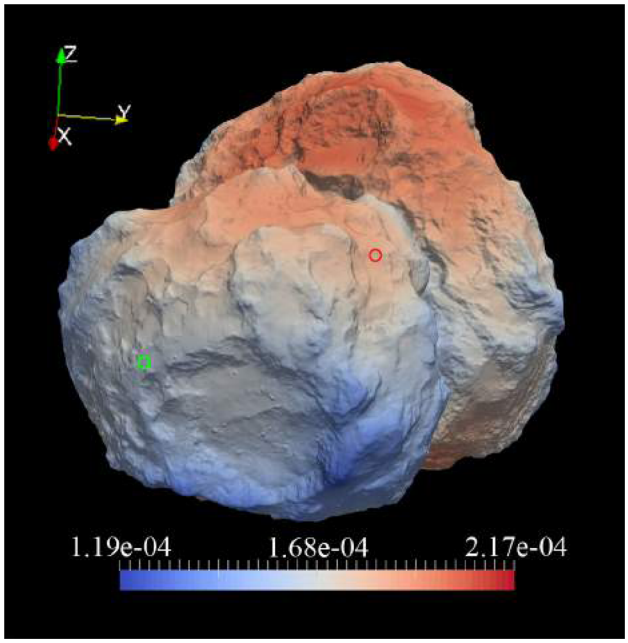

Figure 2. Gravitational map (m s^{-2}) of 67P after taking into account the rotational acceleration. The red circle shows the location of Sais landing site, while the green circle indicates the location of Agilkia landing spot. (For interpretation of the references to colour in this figure legend, the reader is referred to the web version of this article.)

scale of the images we set the lowest statistically significant pebble dimension to 0.07 m, because below this value, the distribution starts to roll over indicating incompleteness of the SFD. In addition, the 0.07 m limit value exceeds the three-pixel sampling rule (Nyquist 1928), providing trustful size-frequency statistics. Since the observations were performed at a phase angle of ∼30.5°, the shadows on the surface provided the possibility of identifying even smaller boulders. Nevertheless, we excluded these smaller boulders for the sake of completeness. This approach is commonly used in boulders identification and analysis, as presented for example in Michikami et al. (2008), Mazrouei et al. (2014) and Pajola et al. (2017).

After identifying all possible boulders/pebbles, the obtained data were then binned with a bin size equivalent to the pixel resolution (Pajola et al. 2016b), i.e. 0.014 m. Then, in order to obtain the pebbles/boulders SFD per m^2, we used the corresponding area computed knowing the FOV extension.

Afterwards, by using the 3D gravitational and rotational models produced by the OSIRIS team (Preusker et al. 2015; Jorda et al. 2016), we computed the gravitational values as in Sierks et al. (2015) of the Sais area and of the Agilkia landing site as well, in order to compare the two areas (see Fig. 2).

3 RESULTS

Following the same surface texture criteria of Giacomini et al. (2016), we have identified three morphological units on Sais (Fig. 3), i.e. (i) an outcropping consolidated terrain, characterized by a dust-coating-free surface that shows a rocky appearance, (ii) a coarse boulder deposit, where clusters of pebbles/boulders are evident with a distinct granular aspect and (iii) a fine particle deposit, that appears smoother than the coarse deposit due to the presence of dusty material intermixed with pebbles and boulders.

Over the considered Sais area (Figs 4 A and B) we counted a total of 4221 pebbles/boulders, 1132 of which on the coarse deposit and 3089 on the fine deposit (see Figs 4 C and D). The spatial distribution of all pebbles/boulders is presented in Figs 4(E) and (F). The largest boulder identified reaches a maximum size ∼0.7 m.

Analysing the Sais data, we preferred to use the differential size distribution with linear bins instead of the commonly used differential size distribution with logarithmic bins (Mottola et al. 2015) because it distributes the data points in a similar fraction around the knee (Figs 5 and 6), thus providing the best estimate of the power-law index best fitting the data below and above the knee. Consequently, the power-law index of the differential distribution with linear bins can be easily converted to that with logarithmic bins, and to that of the cumulative distribution, by adding one. The (cumulative) power-law index that results from this conversion must be negative in order to be valid.

The resulting pebbles/boulders SFD computed over the entire Sais study area is presented in Fig. 5. The distribution is best fitted by a two-segment power-law joint by a 'knee' at size s_k: the first segment ranges between 0.07 and 0.26 m, and has a differential power-law index of -1.7 ± 0.1, the second one ranges between 0.26 and 0.50 m, and has a differential power-law index of -4.2 $+0.4/-0.8$ (for the method see e.g. Lamy et al. 2004; Lamy & Toth 2009; Snodgrass et al. 2011). The density of pebbles with a size of 0.07 m is 2.56 m^{-2}, while with a size of 0.26 m is 0.34 m^{-2}.

We then separated the pebbles/boulders located on the coarse deposit from those on the fine one in order to quantify the size-frequency differences between the two units. By looking at Figs 6(A) and (B), it is evident that both the coarse and the fine deposits are characterized by a clear change in slope at $s_k \sim 0.26$ m. Below this value the fine deposit is fitted by a power-law index of -2.0 $+0.1/-0.2$, while above 0.26 m its best fit is a power-law curve with index of $-4.7+0.6/-0.8$. The density of pebbles with size 0.07 m is 2.99 m^{-2}, and 0.29 m^{-2} at a size of 0.26 m (we recall that the width of the size bin is 0.014 m and the density applies to all types of sizes within the bin centred on those values). Contrarily, at the bigger pebbles/boulders dimensions the coarse deposit is fitted with a power-law index of -3.8 $+0.5/-0.7$. Instead, below 0.26 m, even when considering only those values above 5 pixels, a decrease of pebbles/boulders is evident. Despite the scatter of the data that makes the fitting challenging, we tentatively fitted them with a power-law curve that returns an index of -0.9 ± 0.1. The

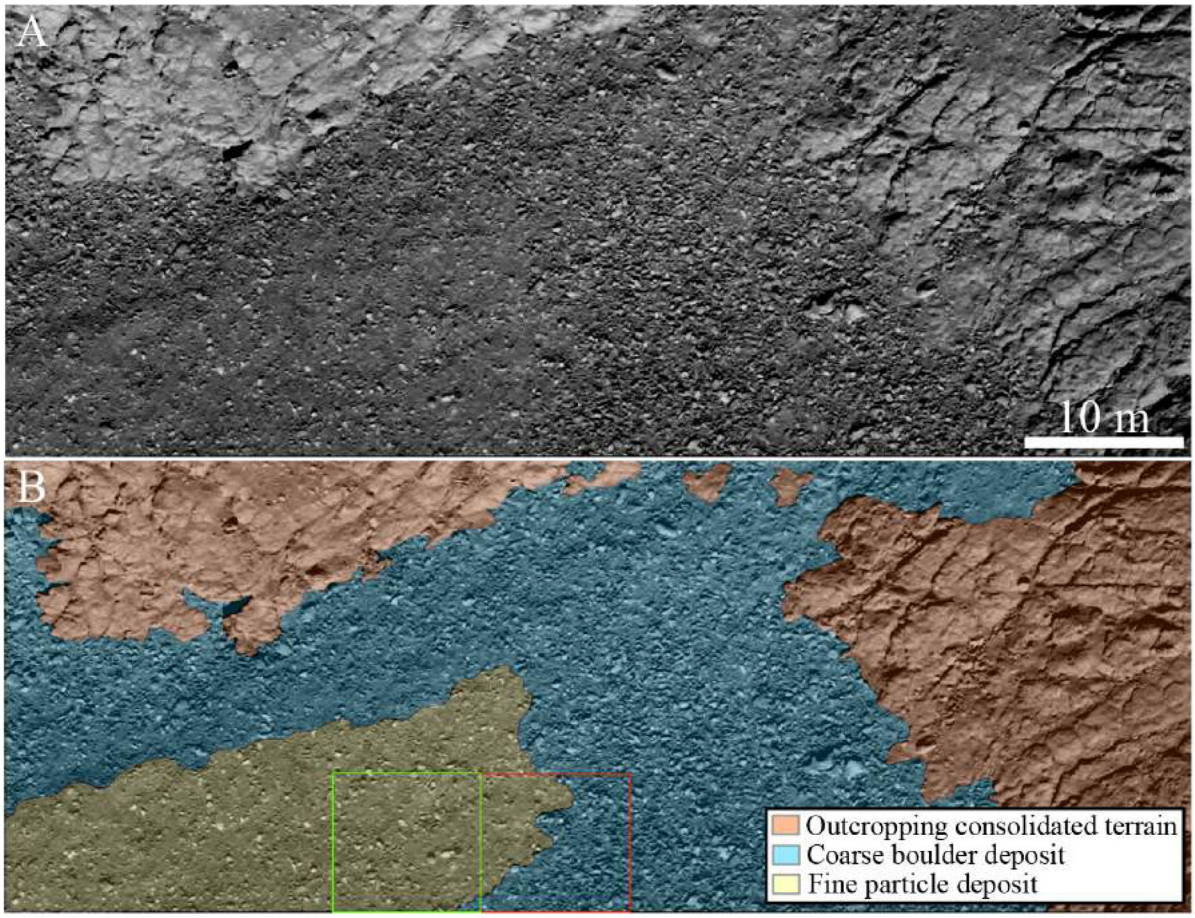

Figure 3. (A): WAC image taken on 2016 September 30 at 10:29:08 UT 452 m from the nucleus surface. (B): morphological map showing the three different units identified on Sais. The green and red squares show the extension of Figs 4(A) and (B). (For interpretation of the references to colour in this figure legend, the reader is referred to the web version of this article.)

density of pebbles with size 0.07 m is 1.36 m^{-2}, i.e. 2.2 less than the fine deposit, and 0.43 m^{-2} at the size of 0.26 m, i.e. 1.48 times than the fine one.

4 DISCUSSION AND COMPARISON BETWEEN SAIS AND THE AGILKIA SITE

Previous analyses performed at different locations of 67P (La Forgia et al. 2015; Pajola et al. 2015; Pommerol et al. 2015; Vincent et al. 2015, 2016; Deshapriya et al. 2016; Pajola et al. 2016b,c; Lucchetti et al. 2016; Oklay et al. 2016, 2017) showed that the cumulative SFDs for boulders >1 m can be fitted through power-law curves. Different origins or evolution processes of the studied boulder fields result in different power-law indices, such as (i) the −5.0 to −6.5 range in the case of the formation of a pit after ceiling collapse, with a boulder field at its bottom; (ii) the −3.5 to −4.5 range, when taluses below receding cliffs are analysed, or (iii) the −1.0 to −2.0 range derived on degraded boulders through sublimation located in the middle of wide depressions, not being replenished by the distant retreating walls (Pajola et al. 2016b).[4]

Only for the Agilkia case, the resolution of the ROLIS images captured during Philae's landing provided the possibility to study the cometary regolith at the centimetre and decimetre scale (Mottola et al. 2015, Fig. 7). We made use of the Mottola et al. (2015) data set (we did not recount the pebbles/boulders on Agilkia), and consequently identified the SFD of the airfall population both in the smooth and rough units, once again derived through a power-law fitting of the pebbles/boulders data set. When grouped with a linear bin size in the differential representation, the resulting power-law index for the Agilkia smooth unit is −3.8 +0.2/−0.3 (Fig. 8 A), while on the rough deposit it is −3.4 +0.4/−0.5 in the size range 0.05–0.28 m, and −4.3 ±0.5 at sizes above 0.28 m, Fig. 8(B) (we recall that the difference of 1 with respect to the Mottola et al. 2015 results is due to the use in this analysis of the linear bin, instead of the logarithmic one).

Since the considered WAC Sais data set has a similar scale to the ROLIS one (the last image of ROLIS data set being taken at a distance of 9 m, with a pixel scale of 0.95 cm $pixel^{-1}$, see table 1 of Pajola et al. 2016a), we decided to compare the SFD of the two landing areas. The resulting Fig. 7 depicts a clear texture difference between the two sites. The Agilkia site is dominated by a ubiquitous

[4] We recall that the values presented in (i), (ii) and (iii) were derived on cumulative SFDs. Therefore the corresponding differential power-law indices using a linear bin size are equivalent to the cumulative values minus 1, i.e. a cumulative −3.5 power-law index is equivalent to a differential −4.5 one.

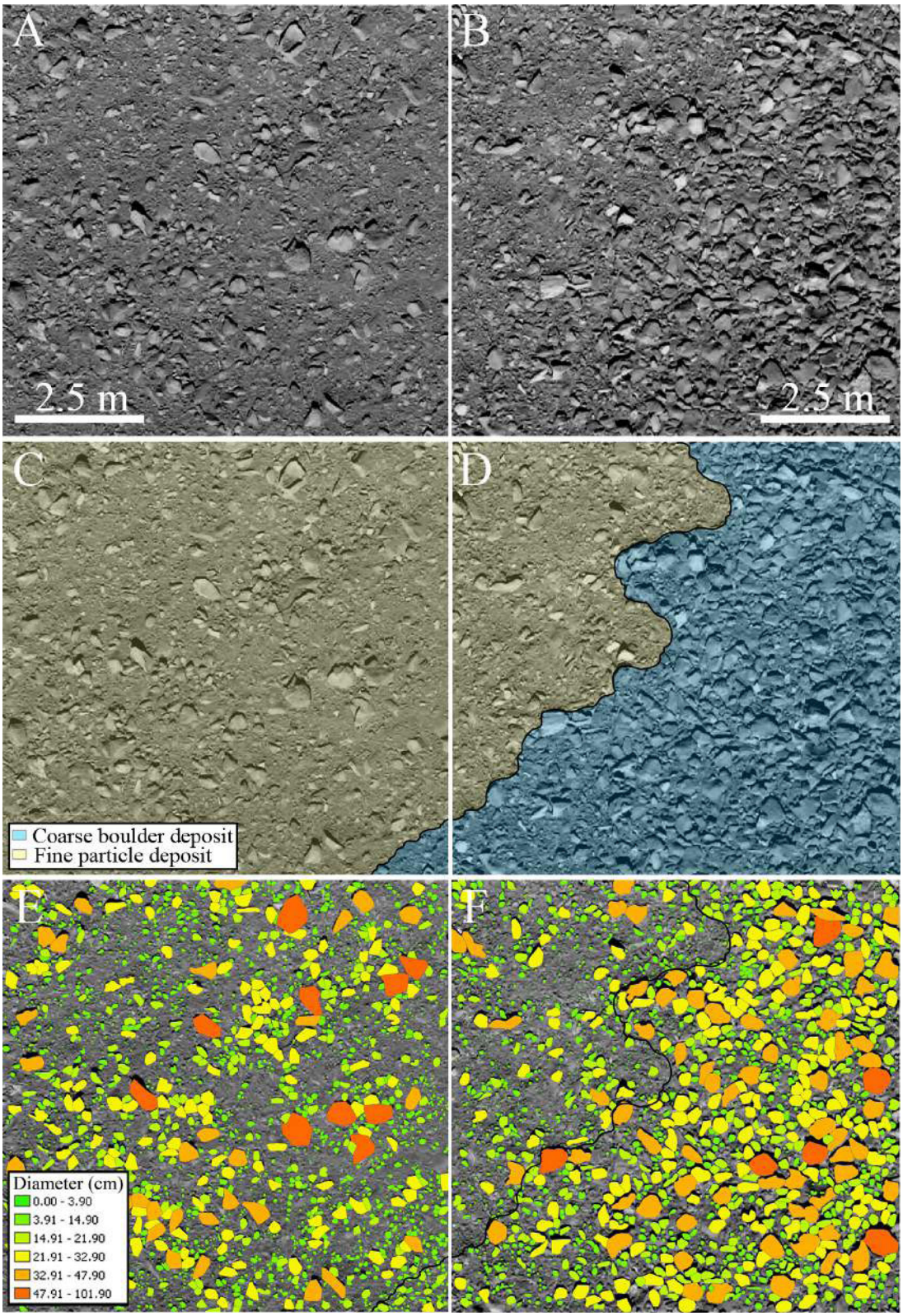

Figure 4. (A): WAC image taken on 2016 September 30 at 10:36:55 UT 138 m from the nucleus surface. (B): WAC image taken on 2016 September 30 at 10:37:04 UT 130 m from the nucleus surface. (C) and (D): morphological maps showing the two pebbles/boulders textures on Sais. (E) and (F): the spatial distribution of the pebbles/boulders identified on the WAC images. The pebbles/boulders are classified on their different sizes. (For interpretation of the references to colour in this figure legend, the reader is referred to the web version of this article.)

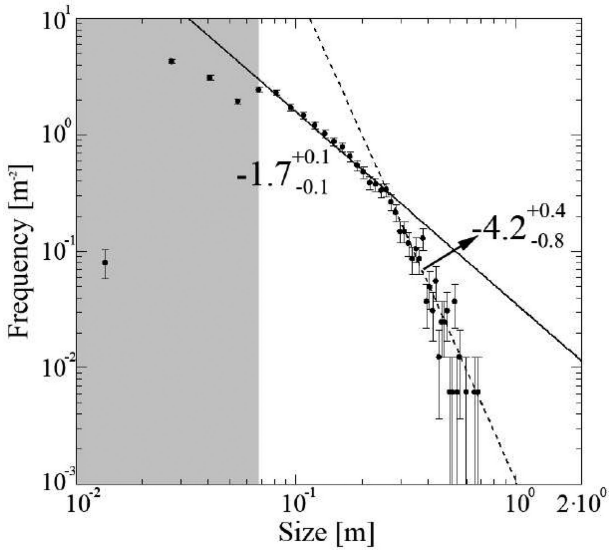

Figure 5. The pebble/boulder differential SFD per m^2 identified on the Sais study area of Figs 4(A) and (B). The grey area contains all values detected below 5 pixels. The two black lines are fitted regression interpolation of the data computed in the range 0.07–0.26 m (continuous line, returning a power-law index of -1.7 ± 0.1) and in the range 0.26–0.50 m (dashed line, returning a power-law index of -4.2 $+0.4/-0.8$). Vertical error bars indicate the root of the frequency, divided by the area computed knowing the FOV (this is valid for all other plots presented in this work). The bin size is 0.014 m.

presence of a cm-sized debris blanket that covers partially, if not entirely, the bigger boulders. On the contrary, this blanket is not observed on the Sais area, where the presence of larger and more frequent pebbles/boulders is evident.

Why is the Sais site deposit so different with respect to the Agilkia one?

All the distributions in Figs 5, 6 and 8(B) show a similar behaviour, i.e. a steep distribution above $s_k \approx 0.3$ m, with a differential power-law index consistent with ≈ -4.2. The data at sizes >0.3 m of the Agilkia smooth terrain are consistent with this description as well. On the contrary, the power-law index below the knee s_k has significantly different values, strongly correlated with the abundance of deposits composed by pebbles too small to be resolved by ROLIS and OSIRIS. We name this unresolved deposit as fine deposit, composed of particles smaller than 1 cm. We conclude that the power-law index below s_k depends on the thickness of the fine deposit: when it is very thick, it buries all largest pebbles, providing a very steep power-law index, −3.8, like in Agilkia smooth terrains. The thinner the fine deposit, the shallower the size distribution below s_k is, with the limit case of coarse terrains in Sais, where the index approaches zero.

The activity of 67P along its orbit provides a coherent scenario of how all these deposits were formed. The radius of the largest ejectable particle is proportional to the lift pressure, i.e. the product $Q_w \times v_w$, where Q_w is the water production rate per unit surface area and v_w is the water ejection speed (Wallis 1982). It depends also on the local gravity, which however, as shown in Fig. 2, changes by a factor of 2 over the entire comet only, so it can be neglected here. Fig. 9 shows that the variation of lift pressure is orders of magnitudes larger. We computed the lift pressure for different regions on 67P by using the thermophysical model described in Keller et al. (2015).

Fig. 9 shows that at perihelion (1.24 au), a southern region like Bes (see El-Maarry et al. 2016 for its geographical location) is the main producer of dust of any size. OSIRIS observations have shown that this region ejects chunks up to the radius of 0.4 m out of the comet gravity field (Fulle et al. 2016b).[5] However, due to the non-spherical nucleus shape of 67P, much larger boulders may be lifted-up from the nucleus surface, because the radial decrease of the gas density may be locally much faster than that of the nucleus gravity field. Marschall et al. (2016) compute that the largest boulders that are marginally lifted-up are about 25 times larger than those not affected by any gravity selection. Fulle et al. (2016b) and Ott et al. (2017) find no evidence of such a selection up to a radius of $r = 0.2$ m, so that 67P gas drag can probably lift up chunks up to a radius of ≈5 m, that however cannot escape the nucleus gravity field. Probably, boulders with a radius just larger than 0.2 m may be distributed over all the nucleus surface, whereas boulders of radius just below 5 m fall very close to the ejection point.

We start to consider the airfall on Hapi (see El-Maarry et al. 2015 for its geographical location) of the material ejected by Bes. Hapi, located on the northern hemi-nucleus, around perihelion has a polar night longer than Sais (Fig. 9), so that Hapi's airfall is composed both of a fine deposit thicker than Sais', and of boulders up to sizes of ≈10 m (the steep size distribution makes their number low). We do not have images of the Hapi deposits with a resolution similar to the one we have on Sais or Agilkia. For this reason the size distribution of Hapi's deposits cannot be directly measured. We therefore assume that this distribution is described by the size distribution on the nucleus surface inferred from coma data collected before perihelion, which is in fact dominated by the dust ejected from Hapi (Della Corte et al. 2015; Thomas et al. 2015a). This differential size distribution has a power-law index close to −2 below 0.1–1 mm (the size uncertainty is due to the conversion from the dust mass measured by GIADA to the dust cross-section measured by OSIRIS), and to −4 above Rotundi et al. (2015); Fulle et al. (2016b). At 2.5 au outbound, the airfall stops, because the gas drag from Hapi overcomes that from Bes. However, since the lift pressure is $\approx 10^4$ times lower than in Bes, Hapi's activity can eject particles of size $\approx 10^4$ times lower than that ejected by Bes, i.e. dust of size <0.1 mm with high efficiency (escaping the nucleus gravity), and with much lower efficiency dust <1 mm (falling mostly around the ejection spot). This explains the pre-perihelion dust size distribution observed to come from Hapi by GIADA and OSIRIS (Rotundi et al. 2015; Della Corte et al. 2015; Fulle et al. 2016b), with a knee at about 0.1–1 mm and a much shallower index (−2) below 0.1 mm than above 1 mm (−4). The index observed above s_k is consistent with the index above s_k observed both in Agilkia and Sais, and with the power-law index above 1 mm extracted by models of ground-based observations of trails, tails and 67P coma (Fulle et al. 2010; Moreno et al. 2016).

On the contrary, the perihelion polar night of Sais is much shorter than the one of Hapi, and this explains the extremely thin fine deposits on Sais, as shown by their shallow size distribution, implying a low number of pebbles composing them. These thin deposits are easily eroded, exposing the coarse deposits characterized by a steeper power-law index close to −4.2 above the knee size. When the airfall from Bes to Sais stops (at heliocentric distance >2.1 au), Sais' lift pressure, a factor 50 below Bes' at perihelion, cleans up

[5] In Bertini et al. (2015), no objects in bound orbits larger than 1 m have been identified between 20 km and 100 km from the nucleus, while no unambiguous detections of objects in bound orbits larger than 6 m have been identified within 20 km far from the comet. This supports the fact that no ejected chunks with diameter bigger than few metres leave 67P's surface.

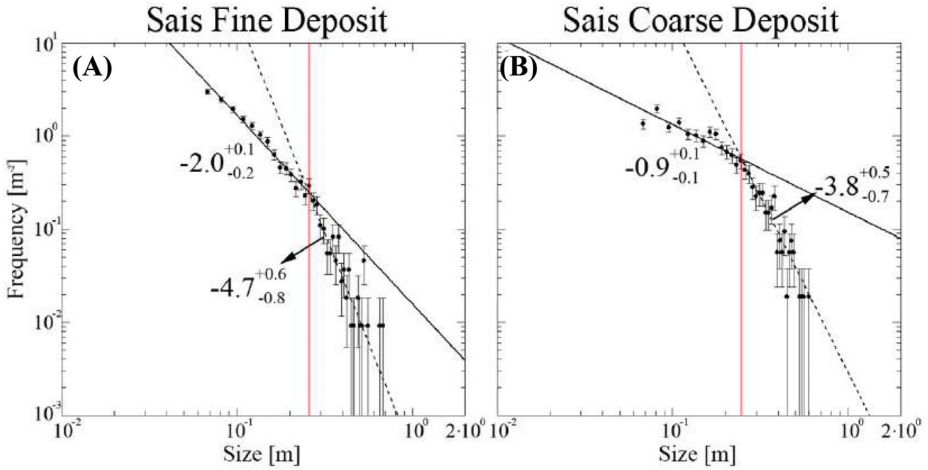

Figure 6. The pebble/boulder differential SFD per m^2 identified on the fine particle deposit (A) and on the coarse boulder deposit (B) of Sais, as shown in Figs 4(C) and (D), respectively. The red lines in A and B indicate the knee of the distribution present both in the fine and coarse deposit. The bin size is 0.014 m. (For interpretation of the references to colour in this figure legend, the reader is referred to the web version of this article.)

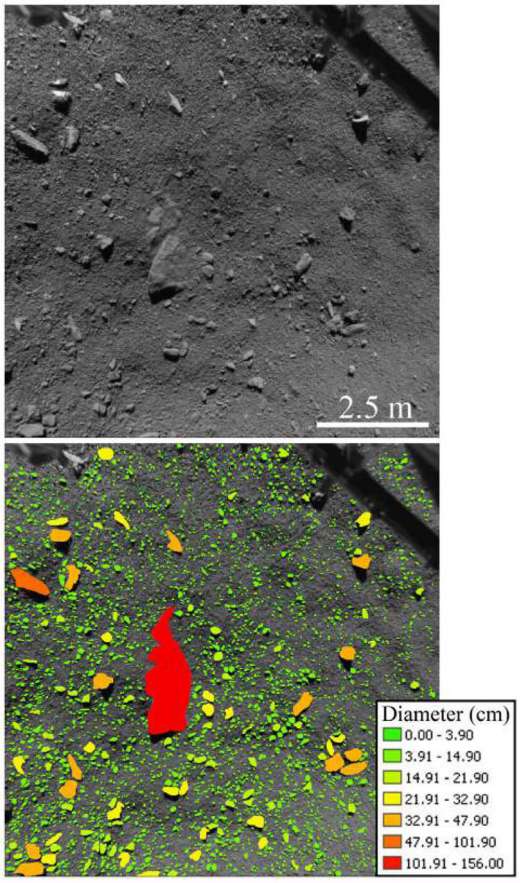

Figure 7. The spatial distribution of the pebbles/boulders identified on Agilika (ROLIS images). This is a reproduction taken from Pajola et al. (2016a), and based on the counts of Mottola et al. (2015). None the less, in order to help the comparison with the Sais counts of Fig. 4, the pebbles/boulders are classified on their different sizes with the same ranges in both areas. The resolution of the Agilkia and Sais images is comparable (0.010 m for Agilkia and 0.014 m for Sais). We recall that the ROLIS image was taken when the comet was at 3.0 au inbound, while the WAC data set was taken when the comet was at 3.82 au outbound. (For interpretation of the references to colour in this figure legend, the reader is referred to the web version of this article.)

Sais of all the dust of ≈2 cm, and with much lower efficiency up to the size s_k ∼0.26 m. This size range corresponds to the shallow size distribution in Sais below s_k, with very small power-law indices because Sais activity has almost completely (in the coarse terrains) or largely (in the smooth terrains) eroded the fine deposits fallen at perihelion. Moreover, in this case the size distribution above s_k corresponds to that of the pristine material ejected from Bes. Agilkia has no polar night, so that its perihelion airfall is composed only of pebbles of size >0.1 m, which, falling on Agilkia fine deposits, erodes them around all the boulders, forming the wind-tails observed to come from south (Mottola et al. 2015). The fine deposit cannot be formed at perihelion, because Agilkia's activity does not allow such a fine airfall. Agilkia's fine deposits must therefore have come from Hapi, during the inbound 67P orbit, when Hapi's lift pressure is much larger than in Agilkia. The thickness of these fine deposits from Hapi to Agilkia is thicker than those on Sais, as shown by the steeper size distributions of fine deposits in Agilkia versus Sais, of differential power-law index <−3.4 versus >−2, probably because the airfall from Hapi lasts much longer than Sais perihelion polar night; it may be however thinner than in Hapi, because the ejection rate from Hapi is orders of magnitude lower than from Bes at perihelion. If Hapi's fine deposits are instead thicker than Agilkia's ones, then the shallower power-law index of fine deposits in Hapi versus Agilkia may be due to selection effects affecting Hapi's largest ejected dust.

At Philae's landing, Agilkia's lift pressure is a factor 50 lower than in Bes at perihelion, so that Agilkia's activity erodes with high efficiency all the fine deposits of size <2 cm, and with less efficiency all pebbles of size $<s_k$. The lift pressure from Agilkia at Philae's landing is close to the maximum one from Sais (at 2.1 au outbound). This explains the similar s_k values in Figs 6 and 8. Again, the Agilkia power-law index above s_k corresponds to that of the pristine material ejected by Bes at perihelion. Pajola et al. (2016a) assumed a differential power-law index of −3.7 in the mass range from 1 to 100 kg of the material ejected by 67P at perihelion. The new results obtained here show that in this mass range the differential power-law index of the material ejected by 67P at perihelion is steeper, close to −4.2, and consistent with the output of trail, tail and coma models applied to ground-based observations (Fulle et al. 2010; Moreno et al. 2016). This does not affect the measured dust loss rate at perihelion of about 8×10^3 kg s^{-1}

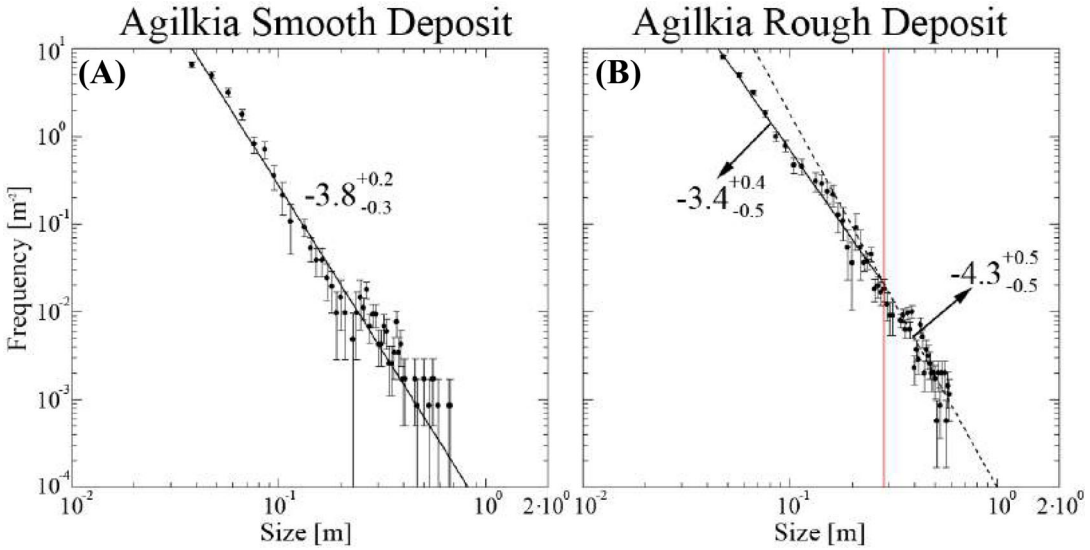

Figure 8. The pebbles/boulders differential SFDs per m^2 identified on the two units present on Agilkia, i.e. the so-called Smooth (A) and Rough deposits (B). The vertical red line in B indicates the knee of the distribution present on the rough deposit. We here underline that the data used are those of Mottola et al. (2015) but with linear bins. (For interpretation of the references to colour in this figure legend, the reader is referred to the web version of this article.)

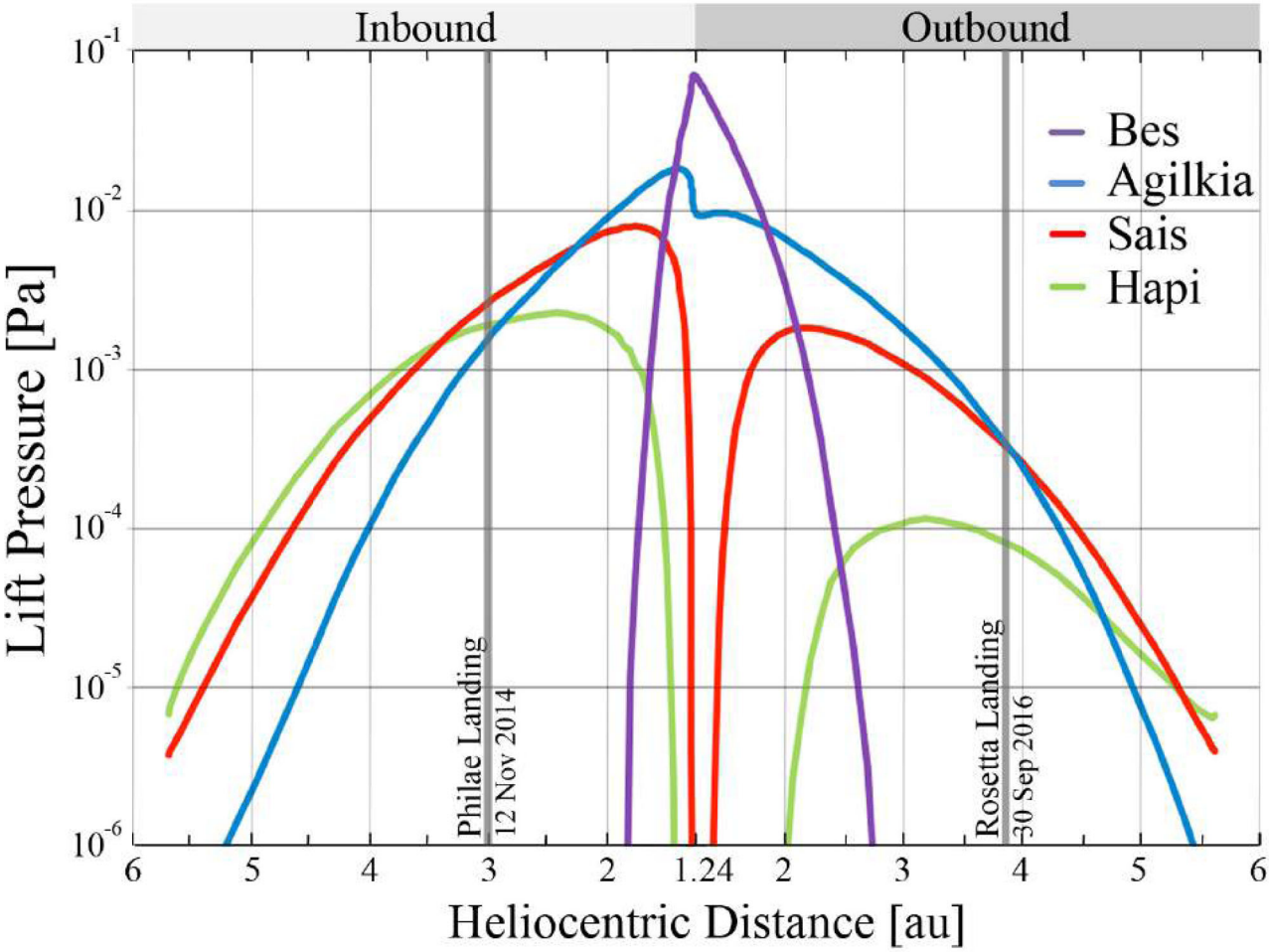

Figure 9. Time evolution of the lift pressure computed for four different locations on 67P at different distances from the perihelion, both inbound and outbound. The perihelion distance of 67P is at 1.24 astronomical unit, au. (For interpretation of the references to colour in this figure legend, the reader is referred to the web version of this article.)

(Fulle et al. 2016b), a value confirmed by Ott et al. (2017), which implies a dust-to-gas ratio close to 20, much larger than the value around 3 measured by RSI (Paetzold et al. 2016). This suggests that most of the pebbles and boulders ejected at perihelion are falling back into the northern deposits as discussed in this section. The relationship between the dust-to-gas ratio observed in the ejected material, in the deposits and inside the nucleus is complex, and consistent with a dust-to-ice mass ratio ≈8 inside 67P, as discussed by Fulle et al. (2017).

5 CONCLUSIONS

We made use of three OSIRIS WAC images taken by *Rosetta* during its final descent towards the surface of comet 67P. These images were taken on 2016 September 30 at a distance range between 450 and 130 m and with a scale of 4.6–1.3 cm pixel^{-1}. With this data set we prepared a high-resolution morphological map of the *Rosetta* Sais final landing site, identifying an outcropping consolidated terrain unit, a coarse boulder deposit and a fine particle deposit. We then derived the pebbles/boulders SFD of the whole area in the size range of 0.07–0.70 m, obtaining a best fit on the entire Sais area with a two-segment power law. The first segment ranges between 0.07 and 0.26 m and has a differential power-law index of −1.7 ±0.1, while the second one ranges between 0.26 and 0.50 m and has a differential power-law index of −4.2 +0.4/−0.8.

When the fine and the coarse particle deposits are considered as separated, we still get two different power-law indices, separated at the 'knee' size value of 0.26 m. Below this value the fine deposit is fitted by a power-law index of −2.0 +0.1/−0.2, while above that its best fit is a power-law curve with index of −4.7+0.6/−0.8. Contrarily, for sizes <0.26 m the coarse deposit is best fitted with a power-law index of −0.9 ±0.1, while above 0.26 m the best fit is a power-law index with value −3.8 +0.5/−0.7. Compared to the Agilkia ROLIS images, the Sais surface is almost entirely free of the ubiquitous, cm-sized debris blanket that was observed during Philae's descent. Nevertheless, the differential SFD computed on the smooth and rough units identified on Agilkia, show a similar trend with a steeper distribution above ∼0.3 m, and a flatter trend below such value.

The activity of 67P along its orbit provides a coherent scenario of how these deposits were formed. In the case of Agilkia, the layer of fine deposits observed by ROLIS at 3.0 au are coming from Hapi, during the inbound 67P orbit, i.e. when Hapi's lift pressure is much larger than the one in Agilkia. The thickness of these fine deposits from Hapi to Agilkia is thicker than the one on Sais, because the airfall from Hapi lasts much longer than Sais perihelion polar night. This explains the power-law indices below 0.26 m being steeper in Agilkia than in Sais. On the contrary, when Sais was observed by *Rosetta* at 3.82 au outbound, its activity had almost completely (in the coarse terrains) or largely (in the smooth terrains) eroded the fine deposits fallen at the 2015 perihelion, resulting in an almost fine material-free surface.

ACKNOWLEDGEMENTS

MP and co-authors would like to personally thank the Reviewer, Dr. Stefan Schröder for important and constructive comments that led to a substantial improvement of the paper.

This work is dedicated to the memory of our colleague and friend Michael A'Hearn who sadly left us in 2017 May.

OSIRIS was built by a consortium of the Max-Planck-Institut für Sonnensystemforschung, in Göttingen, Germany, CISAS-University of Padova, Italy, the Laboratoire d'Astrophysique de Marseille, France, the Instituto de Astrofisica de Andalucia, CSIC, Granada, Spain, the Research and Scientific Support Department of the European Space Agency, Noordwijk, the Netherlands, the Instituto Nacional de Tecnica Aeroespacial, Madrid, Spain, the Universidad Politechnica de Madrid, Spain, the Department of Physics and Astronomy of Uppsala University, Sweden, and the Institut für Datentechnik und Kommunikationsnetze der Technischen Universität Braunschweig, Germany. The support of the national funding agencies of Germany (DLR), Italy (ASI), France (CNES), Spain (MEC), Sweden (SNSB) and the ESA Technical Directorate is gratefully acknowledged. We thank the ESA teams at ESAC, ESOC and ESTEC for their work in support of the *Rosetta* mission.

MP was supported for this research in part by an appointment to the NASA Postdoctoral Program at the Ames Research Center administered by Universities Space Research Association (USRA) through a contract with NASA.

We made use of the ARCGIS 10.1 software and IDL to perform the presented analysis.

REFERENCES

Bertini I. et al., 2015, A&A, 583, A19
Della Corte V. et al., 2015, A&A, 583, A13
Deshapriya J. D. P. et al., 2016, MNRAS, 462, S274
El-Maarry M. R. et al., 2015, A&A, 583, A26
El-Maarry M. R. et al., 2016, A&A, 593, A110
Fulle M. et al., 2010, A&A, 522, A63
Fulle M. et al., 2016a, MNRAS, 462, S132
Fulle M. et al., 2016b, ApJ, 821, A19
Fulle M. et al., 2017, MNRAS, 469, S45
Giacomini L. et al., 2016, MNRAS, 462, S352
Jorda L. et al., 2016, Icarus, 277, 257
Keller H. U. et al., 2007, Space Sci. Rev., 128, 433
Keller H. U. et al., 2015, A&A, 583, A34
La Forgia F. et al., 2015, A&A, 583, A41
Lamy P., Toth I., 2009, Icarus, 201, 674
Lamy P. L., Toth I., Fernandez Y. R., Weaver H. A., 2004, in Festou M. C., Keller H. U., Weaver H. A., eds, The sizes, shapes, albedos, and colours of cometary nuclei. Univ. Arizona Press, Tucson, AZ, p. 223
Lucchetti A. et al., 2016, A&A, 585, L1
Marschall R. et al., 2016, A&A, 589, A90
Mazrouei S., Daly M. G., Barnouin O. S., Ernst C. M., DeSouza I., 2014, Icarus, 229, 181
Michikami T. et al., 2008, Earth, Planets, and Space, 60, 13
Moreno F. et al., 2016, A&A, 587, A155
Mottola S. et al., 2015, Science, 349, 020232
Nyquist H., 1928, Trans. Am. Inst. Elect. Eng., 47, 617
Oklay N. et al., 2016, MNRAS, 462, S394
Oklay N. et al., 2017, MNRAS, submitted
Ott T. et al., 2017, MNRAS, in press
Paetzold M. et al., 2016, AAS/Division for Planetary Sciences Meeting Abstracts, 48, 116.27
Pajola M. et al., 2015, A&A, 583, A37
Pajola M. et al., 2016a, MNRAS, 462, S242
Pajola M. et al., 2016b, A&A, 592, L2
Pajola M. et al., 2016c, A&A, 592, A69
Pajola M. et al., 2016d, A&A, 585, A85
Pajola M. et al., 2017, Nature Astron., 1, 0092
Pommerol A. et al., 2015, A&A, 583, A25
Preusker F. et al., 2015, A&A, 583, A33
Rotundi A. et al., 2015, Science, 347, aaa3905
Sierks H. et al., 2015, Science, 347, aaa1044

Snodgrass C., Fitzsimmons A., Lowry S. C., Weissman P., 2011, MNRAS, 414, 458
Thomas N. et al., 2015a, A&A, 583, A17
Thomas N. et al., 2015b, Science, 347, aaa0440
Tubiana C. et al., 2015, A&A, 583, A46
Vincent J.-B. et al., 2015, Nature, 523, 63
Vincent J.-B. et al., 2016, A&A, 587, A14
Wallis M. K., 1982, in Wilkening L. L., ed., IAU Colloq. 61: Comet Discoveries, Statistics, and Observational Selection. Univ. Arizona Press, Tucson, AZ, p. 357
Wentworth C. K., 1922, J. Geol., 30, 377

[1]*NASA Ames Research Center, Moffett Field, CA 94035, USA*
[2]*INAF Osservatorio Astronomico di Padova, Vic. Osservatorio 5, 35122 Padova, Italy*
[3]*INAF Osservatorio Astronomico di Trieste, Via Tiepolo 11, 34143 Trieste, Italy*
[4]*Deutsches Zentrum für Luft- und Raumfahrt (DLR), Institut für Planetenforschung, Rutherfordstrasse 2, 12489 Berlin, Germany*
[5]*CNR-IFN UOS Padova LUXOR, Via Trasea 7, 35131 Padova, Italy*
[6]*Center of Studies and Activities for Space, CISAS, 'G. Colombo', University of Padova, Via Venezia 15, 35131 Padova, Italy*
[7]*Department of Geosciences, University of Padova, Via G. Gradenigo 6, 35131 Padova, Italy*
[8]*Max-Planck-Institut für Sonnensystemforschung, Justus-von-Liebig-Weg, 3 37077 Göttingen, Germany*
[9]*CNRS LAM (Laboratoire d'Astrophysique de Marseille), Aix Marseille Universite, UMR 7326, 13388 Marseille, France*
[10]*Observatory of the Hungarian Academy of Sciences, PO Box 67, 1525 Budapest, Hungary*
[11]*NASA Jet Propulsion Laboratory, 4800 Oak Grove Drive, Pasadena, CA 91109, USA*
[12]*Department of Information Engineering, University of Padova, Via Gradenigo 6/B, 35131 Padova, Italy*
[13]*Department of Physics and Astronomy 'G. Galilei', University of Padova, Vic. Osservatorio 3, 35122 Padova, Italy*
[14]*Laboratoire d'Astrophysique de Marseille, UMR 7326 CNRS & Aix-Marseille Université, 38 rue Frédéric Joliot-Curie, 13388 Marseille cedex 13, France*
[15]*Centro de Astrobiologa, CSIC-INTA, 28850 Torrejon de Ardoz, Madrid, Spain*
[16]*International Space Science Institute, Hallerstrasse 6, 3012 Bern, Switzerland*
[17]*Scientific Support Office, European Space Research and Technology Centre/ESA, Keplerlaan 1, Postbus 299, 2201 AZ Noordwijk ZH, the Netherlands*
[18]*Department of Physics and Astronomy, Uppsala University, 75120 Uppsala, Sweden*
[19]*PAS Space Research Center, Bartycka 18A, 00716 Warszawa, Poland*
[20]*Institute for Geophysics and Extraterrestrial Physics, TU Braunschweig, 38106 Braunschweig, Germany*
[21]*Department of Astronomy, University of Maryland, College Park, MD 20742-2421, USA*
[22]*LESIA, Observatoire de Paris, PSL Research University, CNRS, Univ. Paris Diderot, Sorbonne Paris Cite and UPMC Univ., Paris 06, Sorbonne Universites, 5 Place J. Janssen, Meudon Principal Cedex 92195, France*
[23]*LATMOS, CNRS/UVSQ/IPSL, 11 Boulevard d'Alembert, 78280 Guyancourt, France*
[24]*Department of Mechanical Engineering, University of Padova, Via Venezia 1, 35131 Padova, Italy*
[25]*UNITN, University of Trento, Via Mesiano, 77, 38100 Trento, Italy*
[26]*Physikalisches Institut der Universität Bern, Sidlerstr. 5, 3012 Bern, Switzerland*
[27]*Laboratory for Atmospheric and Space Physics, University of Colorado, 3665 Discovery Drive, CO 80301, USA*
[28]*Instituto de Astrofisica de Andalucia CSIC, Glorieta de la Astronomia, 18008 Granada, Spain*
[29]*Institute for Space Science, National Central University, 32054 Chung-Li, Taiwan*
[30]*Space Science Institute, Macau University of Science and Technology, Macau, China*
[31]*Operations Department European Space Astronomy Centre/ESA, PO Box 78, 28691Villanueva de la Canada, Madrid, Spain*
[32]*Institut für Datentechnik und Kommunikationsnetze der TU Braunschweig, Hans-Sommer-Str. 66, 38106 Braunschweig, Germany*

This paper has been typeset from a TEX/LATEX file prepared by the author.